Available online at www.sciencedirect.com
ScienceDirect
Quaternary Research 69 (2008) 316–325
QUATERNARY RESEARCH
www.elsevier.com/locate/yqres

# Age constraints on the late Quaternary evolution of Qinghai Lake, Tibetan Plateau

David B. Madsen [a,*], Ma Haizhou [b], David Rhode [c], P. Jeffrey Brantingham [d], Steven L. Forman [e]

[a] Texas Archeological Research Laboratory, University of Texas, 1 University Station R7500, Austin, TX 78712, USA
[b] Qinghai Institute of Salt Lakes, Chinese Academy of Sciences, Xining, Qinghai 810008, PR China
[c] Division of Earth and Ecosystem Sciences, Desert Research Institute, Reno, NV 89512, USA
[d] Department of Anthropology, University of California Los Angeles, Los Angeles, CA 90095, USA
[e] Department of Earth and Environmental Sciences, University of Illinois at Chicago, Chicago, IL 60607, USA

Received 12 March 2007
Available online 26 December 2007

**Abstract**

Dating and geomorphology of shoreline features in the Qinghai Lake basin of northwestern China suggest that, contrary to previous interpretations, the lake likely did not reach levels 66–140 m above modern within the past ~90,000 yr. Maximum highstands of ~20–66 m above modern probably date to Marine Isotope Stage (MIS) 5. MIS 3 highstands are undated and uncertain but may have been at or below post-glacial highs. The lake probably reached ~3202–3206 m (+8–12 m) during the early Holocene but stayed below ~3202 m after ~8.4 ka. This shoreline history implies significantly different hydrologic balances in the Qinghai Lake basin before ~90 ka and after ~45 ka, possibly the result of a more expansive Asian monsoon in MIS 5.


*Keywords:* Tibetan Plateau; Late Quaternary; Climate change; Qinghai Lake; Shoreline geomorphology

## Introduction

Qinghai Lake, on the northeastern Tibetan Plateau margin, is China's largest extant closed-basin lake. Its size and proximity to three major climate systems makes it sensitive to global-scale climate change (e.g., Benn and Owen, 1998; Qin and Huang, 1998; Liu et al., 2002; Hong et al., 2003; Morrill et al., 2003; Lehmkuhl and Owen, 2005; Yu, 2005; Herzschuh, 2006) and it has been the subject of numerous paleoenvironmental investigations, most involving climatic proxies derived from sediment cores. The lake's shoreline history is less well known and chronological details are limited and contradictory. Here we report new age estimates of shoreline, geomorphic, and archaeological deposits that refine the Qinghai Lake shoreline history, with implications for central Asian climate extending back to MIS 5 and possibly earlier.

## Setting and previous research

Qinghai Lake (Fig. 1), located at 100°E, 37°N, with a surface elevation of 3194 m, a maximum depth of 30 m, and an area of 4304 km$^2$ (as of 1983), is the terminus of a moderately high elevation drainage basin (~30,000 km$^2$ area) (Wang et al., 1991; Liu et al., 2002; Shen et al., 2005). The lake derives most of its water from the Qilian Mountains via the Buha River, supplemented by numerous smaller streams. Much of the basin varies between 3200 and 3400 m altitude, but about half exceeds 3600 m and surrounding mountains exceed 4500 m. Regional climate is alpine and continental, with long, cold winters and short, mild summers. Most (~65%) of the ~350–400 mm annual precipitation (at lake level) falls in summer (Qin and Huang, 1998; Yu, 2005). The watershed lies at the fringes of the East Asian and Indian summer–monsoon influences within the regime of prevailing continental dry Westerlies from northern Eurasia (Benn and Owen, 1998; Sheppard et al., 2004; Vandeberghe et al., 2006), as modulated and amplified by the influence of the Tibetan Plateau itself (Lu et al., 2004a,b;

* Corresponding author.
*E-mail address:* madsend@mail.utexas.edu (D.B. Madsen).

0033-5894/$ - see front matter © 2007 University of Washington. All rights reserved.
doi:10.1016/j.yqres.2007.10.013

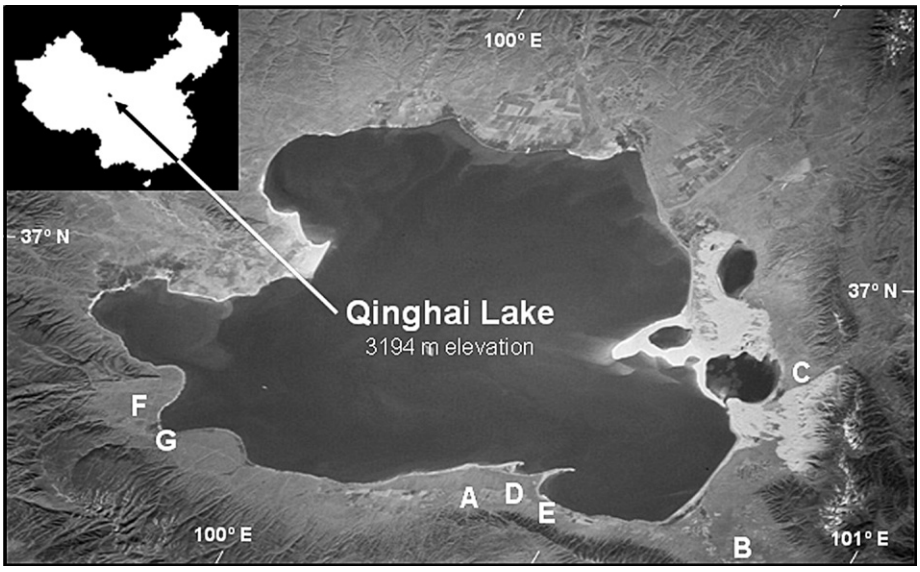


Figure 1. Satellite image of Qinghai Lake showing localities discussed in the text: (A) Ice/sand wedge casts at the head of bajada alluvium near Jiangxigou. (B) Highest shorelines at ~3230–3260 m. (C) Barrier bars on northeastern shore between ~3220 and 3250 m. (D) South shore exposure with ice/sand wedge casts dating to ~22.6 cal ka within bajada alluvium overlying ripple laminated shoreline deposits. (E) South shore exposure at ~3240 m with possible lacustrine deposits bracketed by OSL dates of ~93.3 and 38.8 cal ka. (F) Road cuts ~3205–3210 m through aeolian and possible lacustrine deposits on the southwestern lake margin dating to ~25.0 and 94.5 cal ka, respectively. (G) Archaeological sites Heimahe #1 and #3 in loess at ~3210 and ~3203 m dating to ~13.1 and ~8.4 cal ka, respectively.

Herzschuh, 2006). Fluctuations in the strength and position of these climatic regimes alter the amount of precipitation and hence runoff in the watershed (Ji et al., 2005; Herzschuh, 2006; Herzschuh et al., 2006).

Early- to mid-Pleistocene lakes began to form in the Qinghai basin as tectonism topographically separated it from the Yellow River drainage (Yuan et al., 1990; Geological Survey, 1991; Pan, 1994), but these early lake stands are identified only from well logs and actual lake elevations are unknown (Lanzhou Institute of Geology, 1979). A number of studies (e.g., Chen et al., 1990; Yuan et al., 1990; Lister et al., 1991; Wang and Shi, 1992; Pan, 1994; Zhang et al., 2004) have identified and dated possible high late Pleistocene paleoshorelines at elevations of 70–140 m above the modern surface. Most of these possible high shorelines have been identified at locations along the southern margin of the lake, particularly along a stream near the town of Jiangxigou. Chen et al. (1990) obtained an age estimate of ~38 $^{14}$C ka BP on snail shells (*Radix shanxiensis*) from features at ~3335 m near Jiangxigou. Zhang et al. (2004) report an age of ~34 $^{14}$C ka BP on shell (type not specified) from gravels at 140 m above the modern lake west of Heimahe on the southwestern margin of the lake. A carbonate coating on those gravels produced an age estimate of ~27.2 $^{14}$C ka BP. Wang and Shi (1992) report a date of ~12.1 $^{14}$C ka BP on charcoal from a lens within sand and horizontally bedded gravels they identify as shoreline deposits near the Jiangxigou stream at ~140 m above the present surface. In contrast to these ages, Porter et al. (2001) report luminescence ages of ~44.5 and ~45.5 cal ka from loess lenses within alluvial bajada gravels along the southern margin of the lake at an elevation of ~3315–3220 m (see note Fig. 8). These gravels are overlain by Holocene loess with no evidence of intervening lake deposition. A soil at the top of the gravels dates to ~33.3 cal ka, whereas aeolian sand in an ice wedge cast originating at the surface of the gravels dates to ~15.1 cal ka.

Intermediate shorelines at elevations of 20–70 m above the modern lake have also been widely reported but have even fewer chronological controls. Chen et al. (1990) identified two lake terraces at ~3245 m and ~3218 m above the current surface, with 3245 m localities being by far the most common. However, no dates are available from any of these localities. Wang and Shi (1992) also recognize two intermediate shoreline terraces, one at 20–65 m above the modern lake and one at 7–26 m. Snail shells (*Galba* sp.) in muds in the higher, middle, and lower portions of the 20- to 65-m terrace northwest of Heimahe date to ~6.9, ~5.3, and ~4.8 $^{14}$C ka BP, respectively. A radiocarbon age estimate on a sample collected from a lacustrine facies in the highest portion of the lower 7–26 m terrace near Jiangxigou dates to ~1.9 $^{14}$C ka BP.

Multiple shorelines below 15 m above the modern lake all appear to post-date the last glacial period. However, Porter et al. (2001) suggest alluvial bajada gravels along the southern shore of the lake dating to MIS 3 grade to a lake 14 m higher than at present. Lister et al. (1991) suggest that the lake could not have exceeded 12 m above its current levels during the post-glacial period, whereas Chen et al. (1990) place the maximum post-glacial elevation at 9.5 m higher than at present. This latter estimate is based on a section near Erlangjian on the southeastern margin of the lake at an elevation of 3207 m. The section is composed of undisturbed aeolian sediments on which several soils were formed. Radiocarbon dates from the section suggest the deposits span the Holocene and most of the post-glacial period. Basal portions of the section are dated to ~14.8 and ~11 $^{14}$C ka BP.

Such conflicting reconstructions result in dramatically different interpretations of late-Pleistocene climate histories and are

in conflict with lake histories derived from sediment cores (e.g., Chen et al., 1990; Yuan et al., 1990; Lister et al., 1991; Wang and Li, 1991;Wang et al., 1991; Wang and Shi, 1992; Yu and Kelts, 2002; Shen et al., 2005; Yu, 2005). Yu (2005; see also Yu and Kelts, 2002) suggests that radiocarbon-controlled seismic data and multiproxy data from cores reaching 26 m in length indicate a shallow lake began to form in the basin about 69 ka but remained at elevations much below Holocene levels until ~29 $^{14}$C ka BP. While these age estimates are derived from extrapolated deposition rates based on multiple Holocene age estimates and a single pre-Holocene date, the latter age of 31,290±380 $^{14}$C yr BP on *Rupia* sp. seeds in one of the cores does suggest late MIS 3 lake levels were quite low. Shorelines on the southern margin of the lake during this period may have been as much as 5–6 km to the north and hence at much lower elevations. Between ~29 and ~18.3 $^{14}$C ka BP, the lake began to dry, and by the Last Glacial Maximum (LGM), aeolian sediments in the lake basin suggest the lake may have been dry. Shen et al. (2005) also suggest the lake was much reduced prior to ~18.3 $^{14}$C ka BP and was at very low levels during the LGM with sand being deposited on the lake floor. However, shallow water persisted in at least some of the Qinghai Lake sub-basins at this time (see also Wang and Shi, 1992).

Millennial- to centennial-scale lake level oscillations of <10 m are recorded in several cores dating to the post-glacial, but precise shoreline elevations for these events are not known (Lister et al., 1991; Wang and Li, 1991; Wang and Shi, 1992; Liu et al., 2002; Yu and Kelts, 2002; Shen et al., 2005; Yu, 2005). After ~15 $^{14}$C ka BP, the summer monsoon system began to develop within millennial-scale climate cycles. Three cool intervals at ~13.4–13.0, ~12.0–11.6, and ~11.0–10.4 $^{14}$C ka BP were separated by warmer and more humid periods (Liu et al., 2002; Yu and Kelts, 2002) with higher lake levels corresponding to these warmer periods (Lister et al., 1991; Yu and Kelts, 2002; Shen et al., 2005; Yu, 2005). During the warm/wet events, lake levels rose to a depth of up to 6 m but declined to very shallow levels or even playa conditions in dry periods (Lister et al., 1991; Yu and Kelts, 2002). Significantly warmer and wetter conditions prevailed during the early, middle, and late Holocene (Lister et al., 1991; Liu et al., 2002; Yu and Kelts, 2002; Shen et al., 2005; Yu, 2005), but corollary shoreline elevations are unknown.

## Dating methods and interpretation

We used optically stimulated luminescence (OSL) to date Qinghai Lake shoreline sediments beyond the range of radiocarbon dating and where organic remains were not present (Table 1). The sequence of analysis (infrared [IR] followed by green excitation) preferentially measures feldspar-sourced and then quartz emissions. All ages are determined by IR and green-light excitation overlap at 2 sigma and thus are statistically similar. We favor the ages determined by green light because quartz is a well-known and robust geochronometer, although of less temporal utility than feldspar (Prescott and Hutton, 1994). As a result, with two exceptions, we use the green ages for interpretive purposes. However, because of the concordance of IR and green ages, when green excitation yields infinite ages, the finite IR age is considered an appropriate age estimate, and for samples UIC 1651 and UIC1829, we use IR ages for interpretive purposes. We used radiocarbon age determinations to supplement these OSL ages where possible. With one exception, their interpretation is straightforward. Beta 219964 (41,010±490) is at the limit of ages determined by the radiocarbon method, and we consider ages older than 40 ka to be possibly of infinite age. As a result, we interpret this date to be equal to or greater than about 45 ka.

Luminescence dating of sediments was completed on the fine-grained (4–11 μm) polymineral and coarse grained (100–250 μm) quartz fractions. Various OSL dating procedures were used to test the internal consistency of the respective ages. All samples were dated by the multiple aliquot regeneration (MAR) dose procedures, using the component-specific dose normalization (CSDN) method (Forman and Pierson, 2002; Jain et al., 2003). This method compensates for sensitivity changes from irradiation and subsequent preheating, rendering robust equivalent dose values. Initially, the CSDN procedure determined equivalent dose with IR stimulation, and subsequently with green light excitation. The fine-grained polymineral extract was also analyzed by the multiple aliquot additive dose (MAAD) methods, under infrared stimulation (880±80 nm), by an automated Daybreak 1100 reader (Forman and Pierson, 2002; Jain et al., 2003). MAR analyses were completed under green (514±20 nm) or blue (470±20 nm) light excitation by a Daybreak reader. The resultant blue emissions were measured at ~ 25 °C by a photomultiplier tube coupled with one 3-mm-thick Schott BG-39 and one 3-mm-thick Corning 7-59 glass filter; these emissions are the most suitable as a chronometer (Balescu and Lamothe, 1992; Lang et al., 2003). The background count rate for measuring emissions was <100 counts/s, with a signal-to-noise ratio of >20. A sample was excited for 90 s, and the resulting emissions were recorded in 1 s increments.

A critical analysis for luminescence dating is the dose rate, which is an estimate of the sediment exposure to ionizing radiation during the burial period. Most ionizing radiation in sediment is from the decay of isotopes in the U and Th decay chains and $^{40}$K, which was determined by inductively coupled plasma mass spectrometry. A small cosmic ray component is included in the estimated dose rate (Prescott and Hutton, 1994). The dose rate also compensated for moisture content estimates at each site.

With one exception, the OSL ages are stratigraphically and chronologically consistent. The age estimate for sample #UIC1827IR is much younger than a variety of both OSL and radiocarbon age determinations made by ourselves and others for overlying alluvium and is inconsistent with other OSL ages for the same depositional unit. The sample was collected from sands immediately underlying large alluvial cobbles that may have affected the total dose rate for the sample. For these reasons, we discount this age in our interpretations.

## Reported high elevation paleoshorelines, 3260–3335 m

Possible high shorelines are reported mainly along the southern lake margin, but we found no evidence for any in the

Table 1
Optically stimulated luminescence (OSL) ages and associated chronologic data for sediments from Qinghai Lake area, China

| Field number | Laboratory number | Equivalent dose (Gy) | A value [e] | Uranium (ppm) [f] | Thorium (ppm) [f] | $K_2O$ (%) [f] | Cosmic dose (mGy/yr) | Total dose rate (mGy/yr) [g] | OSL age (yr) [h] |
|---|---|---|---|---|---|---|---|---|---|
| FS06-05 | UIC1829Ir [b, d] | 277.71±0.18 | NA | 1.2±0.1 | 5.3±0.1 | 2.42±0.02 | 0.25±0.02 | 2.71±0.10 | 102,500±7835 |
| FS06-45 | UIC1830Gr [a] | 90.28±1.02 | 0.07±0.01 | 1.9±0.1 | 8.4±0.1 | 2.13±0.02 | 0.28±0.03 | 3.62±0.15 | 25,000±1850 |
| FS06-45 | UIC1830Ir [b] | 95.74±1.02 | 0.08±0.01 | 1.9±0.1 | 8.4±0.1 | 2.13±0.02 | 0.28±0.03 | 3.71±0.15 | 25,800±1910 |
| FS06-46 | UIC1827Ir [d] | 48.03±1.36 | NA | 1.3±0.1 | 6.4±0.1 | 2.03±0.02 | 0.28±0.03 | 2.58±0.10 | 18,600±1500 |
| FS06-47 | UIC1868Gr [d] | 93.08±0.99 | NA | 1.4±0.1 | 5.2±0.1 | 1.94±0.02 | 0.27±0.03 | 2.40±0.09 | 38,800±2955 |
| FS06-47 | UIC1868Ir [d] | 128.69±0.25 | NA | 1.4±0.1 | 5.2±0.1 | 1.94±0.02 | 0.27±0.03 | 2.40±0.09 | 53,700±4040 |
| FS06-48 | UIC1828Gr | 380.50±2.49 | 0.08±0.01 | 2.5±0.1 | 11.7±0.1 | 1.96±0.02 | 0.21±0.02 | 4.08±0.18 | 93,300±7080 |
| FS06-48 | UIC1828Ir | 377.57±1.28 | 0.06±0.01 | 2.5±0.1 | 11.7±0.1 | 1.96±0.02 | 0.21±0.02 | 3.89±0.18 | 96,900±7355 |
| FS05-35 | UIC1658Ir | 390.47±1.29 | 0.14±0.01 | 2.3±0.1 | 7.3±0.1 | 2.25±0.02 | 0.25±0.02 | 4.13±0.17 | 94,500±7110 |
| FS05-36 | UIC1659Gr | 79.58±0.28 | 0.10±0.01 | 2.6±0.1 | 9.8±0.1 | 2.28±0.02 | 0.27±0.03 | 4.44±0.19 | 17,900±1350 |
| FS05-36 | UIC1659Ir | 79.52±0.28 | 0.10±0.01 | 2.6±0.1 | 9.8±0.1 | 2.28±0.02 | 0.27±0.03 | 4.44±0.19 | 17,900±1350 |
| FS05-36 | UIC1659IrA [c] | 65.15±0.13 | 0.06±0.01 | 2.6±0.1 | 9.8±0.1 | 2.28±0.02 | 0.27±0.03 | 4.05±0.17 | 16,100±1215 |
| FS05-127 | UIC1651Gr | 391.99±2.20 | 0.08±0.01 | 2.4±0.1 | 8.9±0.1 | 2.16±0.02 | 0.29±0.03 | 3.98±0.16 | 98,400±7390 |
| FS05-127 | UIC1651Ir | 391.88±1.21 | 0.06±0.01 | 2.4±0.1 | 8.9±0.1 | 2.16±0.02 | 0.29±0.03 | 3.81±0.16 | 102,900±7755 |
| FS05-166 | UIC1652Gr [d] | 66.92±1.21 | NA | 1.4±0.1 | 6.7±0.1 | 2.51±0.03 | 0.29±0.03 | 2.96±0.11 | 22,600±1790 |
| JXG10E W. | UIC1573IrA [c] | 200.17±0.54 | 0.05±0.01 | 2.6±0.1 | 9.7±0.1 | 3.34±0.03 | 0.31±0.03 | 4.88±0.22 | ≥41,000±3060 |
| JXG10E W. | UIC1573Gr | 223.43±0.34 | 0.05±0.01 | 2.6±0.1 | 9.7±0.1 | 3.34±0.03` | 0.31±0.03 | 4.88±0.22 | 45,600±3390 |

[a] Equivalent dose determined by the multiple aliquot regenerative dose method under green excitation (514 nm) (Jain et al., 2003).
[b] Equivalent dose determined by the multiple aliquot regenerative dose method under infrared excitation (880 nm) (Jain et al., 2003).
[c] Equivalent dose determined by the multiple aliquot additive dose method under infrared excitation (880 nm) (e.g., Forman and Pierson, 2002). Blue emissions are measured with 3-mm-thick Schott BG-39 and one 3-mm-thick Corning 7-59 glass filter that blocks >90% luminescence emitted below 390 nm and above 490 nm in front of the photomultiplier tube. Fine-grained (4–11 μm) polymineral fraction analyzed.
[d] The coarse fraction 150–250 or 100–150 μm quartz fraction is analyzed.
[e] Measured alpha efficiency factor as defined by Aitken and Bowman (1975).
[f] U and Th values calculated from alpha count rate, assuming secular equilibrium. $K_2O$% determined by ICP-MS, Activation Laboratory Ltd., Ontario.
[g] Contains a cosmic rate dose rate component from Prescott and Hutton (1994). A moisture content of 15±5% was assumed, except for UIC1659 with 20±5%.
[h] All errors are at one sigma. Analyses preformed by Luminescence Dating Research Laboratory, Dept. of Earth & Environmental Sciences, Univ. of Illinois-Chicago.

3250- to 3335-m (+56–141 m) elevational range. We examined the putative shoreline features in the +120- to 140-m elevational range for which locational information was available (Chen et al., 1990; Wang and Shi, 1992; Zhang et al., 2004) and they all appear to be of non-lacustrine origin. The age estimates of ~34 $^{14}$C ka BP and ~27.2 $^{14}$C ka BP reported by Zhang et al. (2004) for samples collected at +140 m appear to date alluvial rather than lacustrine deposits, whereas the finely stratified deposits at ~3330 m (+136 m) in the Jiangxigou drainage (Fig. 1A) also appear to be alluvial in origin. Charcoal lenses in sand at the mouth of Jiangxigou canyon dated by Wang and Shi (1992) to 12.1 $^{14}$C ka BP and used to suggest a +120-m-high lake of that age are probably the same as archaeological hearths in dune sand at that location that we excavated and radiocarbon dated to ~ 12.4 $^{14}$C ka BP (Madsen et al., 2006). A supposed wave-cut platform at this elevation is rather the head of a bajada fronting the Qinghai Nan Shan (Porter et al., 2001). We obtained two OSL samples dating to ~45.6 ka and ~98.4 ka from aeolian sand, filling two separate ice/sand wedges formed in this alluvium at the highest point of the bajada (36.5892°N, 100.2928°E), and a limiting AMS date of 19.1 $^{14}$C ka BP (~22.9 cal ka) from intrusive organic material (Table 2). Together these age estimates suggest the wedges formed sometime around or before 40 ka, with the top of the fan deposited before 45 ka and possibly as early as ~100 ka. Ice and/or sand wedge casts are widely scattered in the basin in and on late Quaternary alluvium. Some of these were identified by Porter et al. (2001) as ice wedges, but others may be sand wedges and all these features will require further study to determine their origin.

Exposures at lower elevations on the same bajada contain both multiple soils (e.g., 36.6162°N, 100.3172°E) developed on alluvium and multiple episodes of periglacial activity, suggesting a prolonged period of alluviation alternating with episodes of landscape stability. We found no evidence of lacustrine deposition dating to younger than ~45 ka in numerous 5–10 m deep exposures at mid-elevations (3240–3260 m) or in similar exposures from as low as 3216 m. From one exposure (Fig. 1D), we obtained an OSL date of ~22.6 ka on aeolian sand filling one of a set of ice/sand wedge casts originating from a surface within the bajada alluvium (Fig. 2). In a second exposure (Fig. 1E) we obtained an OSL age of ~38.8 ka on a sample from a sand lens near the base of bajada alluvium overlying possible shoreline lacustrine deposits. The gravels are overlain by Holocene loess with no evidence of intervening lake

Table 2

| Location | Lab number | Material/setting | $^{14}$C yr BP | Cal yr BP |
|---|---|---|---|---|
| Figure 1A | Beta 194540 | Organic sediment in ice wedge cast | 19,080±100 | ~22,927±340 |
| Figure 2B | Beta 219964 | Ostracod shells from lagoon deposits | 41,010±490 | ≥45,000±490(?) |
| Figure 1G | Beta 208334 | Hearth charcoal in surface loess | 7630±50 | ~8410±45 |


Figure 2. Ice/sand wedge casts dating to ~22.6 cal ka within MIS 3 and early MIS 2 bajada alluvium overlying ripple laminated shoreline sands exposed in a south shore gravel pit at ~3246 m (+50 m above modern lake) (36.6012°N, 100.4004°E; Fig. 1D). (1) Blocky, undifferentiated loess with a possible soil ~50 cm from the surface. (2) Coarse alluvium with clasts to 20–30 cm; finer to coarse beds; poorly to moderately sorted; coarse sand lens mixed with cobbles; clay skins on gravel/cobbles at base of unit. (3) Unconformity. (4) Horizontally bedded coarse alluvium with undulating surfaces (slight downward tilt to the west). Contains coarse sand and gravel lenses; cobble clasts reach 10–15 cm. Surface zone of coarse sand and gravel with some weathering (possible soil). (5) Fine-grained sandy near-shore sediments with ripple laminae. Foreset bedding occurs to east of illustrated exposure, oriented east. To the west of illustrated exposure 1.57 m of these lacustrine deposits overlie alluvium of unknown depth. Sediments in lacustrine deposits fine upwards towards center of unit, then coarsen again toward top. Fine sand laminae occur at top and bottom of sequence with ripple laminated fine sand to silt laminae dominant in the middle of unit. Surface has small undulations containing some pebbles and lenses of coarse sand. (A) Ice/sand wedge casts containing coarse aeolian sand and pebbles with vertical orientation following contours of the casts. Casts contain some collapsed gravel sidewalls. Some soil development at surface. An OSL sample 3.92 m below surface was collected from the center of the cast.

deposition. These dates provide confirmation for luminescence ages of ~44.5 and ~45.5 ka on loess lenses within alluvial bajada gravels and ~33.3 and ~16.9 ka on overlying soils (Porter et al., 2001), as well as a $^{14}$C date of ~43.2 ka on aeolian deposits near the southeastern shoreline (Yuan et al., 1990).

Given the age of this alluvial sequence, the absence of lacustrine sediments <45 ka in any of the numerous exposures examined, the lack of shoreline features above 3260 m on steep slopes not covered by alluvium, and the age estimates of intermediate level shorelines discussed below, we conclude there is no evidence for lake highstands 66–141 m above the modern lake surface younger than the terminal mid-Pleistocene.

### Paleoshorelines at ~3215–3260 m

In contrast, shorelines at ~3215–3260 m (+21–66 m) are quite apparent, but dating of these shorelines has been contradictory. Several reportedly date to the Holocene (Chen et al., 1990; Wang and Shi, 1992), but the nature of these landscape features is not clear and/or the relationship between the dated material and their construction is doubtful. The highest Pleistocene shorelines we could identify both in satellite imagery and in field examinations conducted over four seasons of fieldwork are located on the extreme eastern margin of the lake (Fig. 1B). These are characterized by a series of spits, wave-cut benches, and a possible bay mouth bar at elevations of 3250–3260 m (Fig. 3). The elevation of these and other shorelines reported here was estimated using a combination of Chinese government 1:50,000 maps with 10-m contour intervals, barometric instrument readings set to known elevations, and Google Earth imagery. We estimate them to be accurate within ±2 m. The highest shorelines at ~3250–3260 m are as yet undated, but geomorphically they appear to be the same approximate age as the slightly lower shorelines we dated at other locations.

The highest shorelines for which we have direct age controls are at ~3240–3250 m (+46–56 m). These are also the shorelines that are the most well developed, the most extensive, and the most obvious both in imagery and on the ground. On the northeast shore of the lake, a series of barrier bars is obvious in

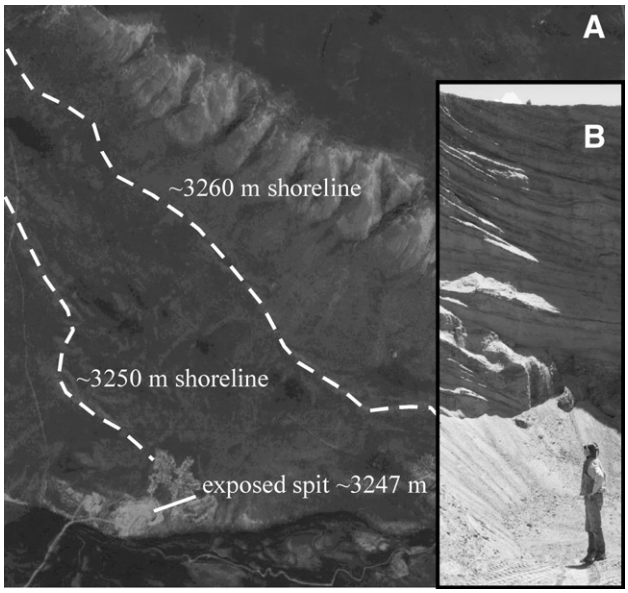


Figure 3. (A) Satellite image of wave-cut benches at the highest late Pleistocene shorelines at Qinghai Lake ~3260 m (+66 m above modern lake) and 3250 m (+56 m) (Fig. 1B). (B) Oblique foreset sands and fine gravels in a small spit exposed in an east shore gravel pit at ~3245–3250 m (+51–56 m) (36.4941°N, 100.8468°E).

satellite imagery (Fig 1C). The highest of these bars is exposed in a road cut at 3245–3250 m (Fig. 4-1). There is no evidence of a higher shoreline at ~3260 m along the north shore of the lake, but the elevational difference may be due to tectonic deformation of the basin, or, more probably, these less well-developed high shorelines are obscured by younger alluvium in these areas. A second barrier bar exposed at ~3235–3240 m (Figs. 1C and 4-2) is built atop alluvium that has a well-defined paleosol on its surface. Horizontally bedded fine-grained lagoonal pond deposits, including a discrete layer of clayey sand, overlie this basal alluvium (Fig. 5). These are overlain, in turn, by a sequence of coarse oblique foreset beach gravels, indicating a transgressive lake phase overtopped the back-beach lagoon. We obtained an OSL age estimate of ~102.5 ka from the horizontally bedded lagoonal sands below the foreset gravels, and a limiting AMS date of ≥41 $^{14}$C ka BP on clean, whole ostracod shells from the clayey sands (Table 2). These dates indicate that the overlying beach deposit is likely older than 90 ka. The top of the foreset gravel is truncated by an erosional unconformity and overlain by post-glacial and Holocene loess. In places, ice/sand wedge casts filled with post-glacial loess extend into the beach gravels.

On the south lakeshore (Figs. 1D, E), surface loess and bajada alluvial gravels overlie ripple laminated near-shore deposits in two gravel pit exposures. At Locality D (Fig. 2), 4 m below the ~3246 m surface, 1.57 m of fine-grained ripple laminated sandy near-shore deposits underlie alluvium dating to MIS 3 and early MIS 2 (see above) and overlie older alluvium of unknown depth. These lacustrine sediments are as yet undated but appear to be equivalent in age to similar deposits at Locality E. At Locality E, lacustrine deposits 4.1 m below the modern surface ~3239 m underlie Holocene loess and MIS 3 alluvium (Fig. 6). An OSL sample from a sand lens near the base of the alluvium 30 cm above the top of the lacustrine sediments and dating to ~38.8 ka provides a bracketing age for this lake excursion. The lacustrine deposits consist of 18 cm of well-sorted coarse beach sand containing unidentified broken shell at the top. These are underlain by a thin unit of ripple laminated silty clay that appear to be lagoonal deposits and 70 cm of sandy near-shore deposits consisting of ripple laminated clayey silt at the base coarsening upwards to fine sand. These, in turn, overlie a second 15-cm-thick unit of medium to coarse well-sorted sand that may also represent beach sand. Laminated silty sand continues to an unknown depth. An OSL sample from 20 cm below the top of the ripple laminated silty sands below the possible lagoonal deposits dates to ~93.4 ka.

Road cuts at elevations of ~3205–3210 m (+11–16 m) on the southwest shore (Figs. 1F and 7) contain a sequence of loess deposition, erosional events, and soil formation overlying fluvial/alluvial sand and gravels with no evidence of intervening


Figure 4. Satellite image of barrier bars on the northeastern shore (Fig. 1C). (A) Highest shoreline at ~3248 m (+54 m). (B) Transgressive shoreline deposit in gravel pit exposure at ~3240 m (+46 m; Fig. 5). (C) Mid-to-late Holocene highstand at ~3202–3 m (+8–9 m).

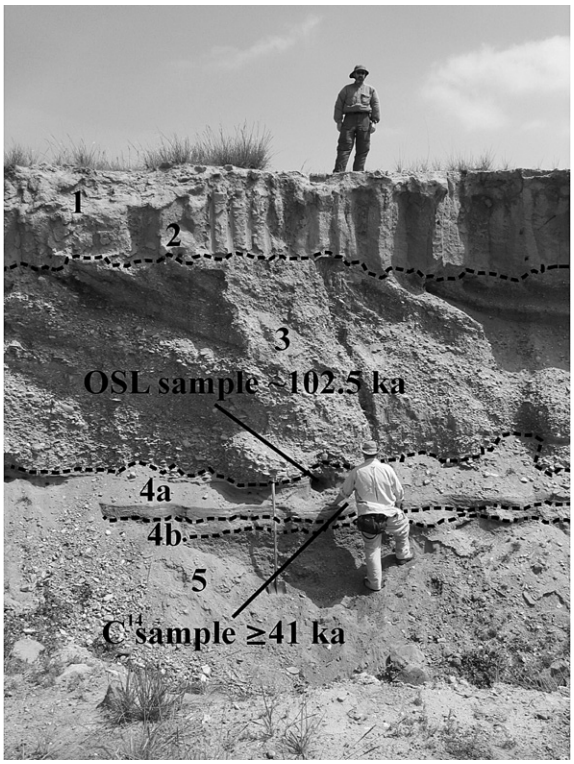


Figure 5. Barrier bar at ~3240 m asl (+46 m above modern lake) exposed in a north shore gravel pit (36.8209°N, 100.7940°E; Fig. 4B). (1) 1–1.4 m blocky loess with incipient soil development on surface. Possible soils at base and middle of unit. (2) Periglacial involutions; loess filled ice wedge casts visible in some areas of gravel pit exposure (but not shown in image). (3) 1.4–4.05 m oblique foreset coarse to medium gravels with some finer sand and gravel stringers. Erosion at surface has produced an unconformity truncating bedding and partially removing a well-developed soil. Clast on clast and clast on matrix support with clasts to 15 cm diameter (3–5 cm average). Foreset bedding trends northeast and gradually extends over underlying lagoonal deposits. (4a) 4.05–4.40 m laminated fine to medium sand. OSL sample collected from center of the unit 4.15 m below surface dates to 102.5 cal ka. (4b) 4.40–4.75 m laminated silty sands grading to finely laminated silty clay containing both ostracods and shell fragments. Clean, whole ostracods from the unit collected 4.50 m below surface date to ≥41 $^{14}$C ka. (5) 4.75 to >8.00 m coarse alluvium with clasts to 20 cm (3–5 cm average) well-developed soil on the surface highly decomposed into pelitized clay.

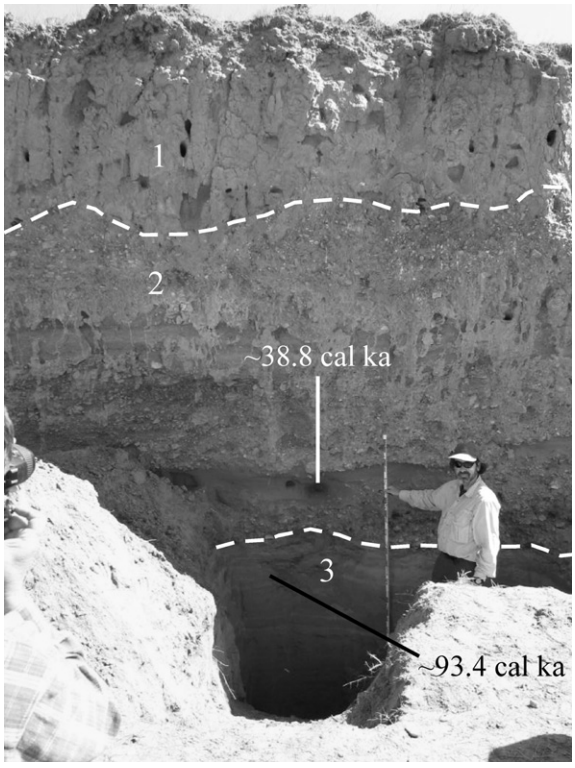


Figure 6. Possible lagoonal deposit below bajada alluvium exposed in south shore gravel pit at ~3239 m (+43 m above modern lake) (36.5959°N, 100.4258°E; Fig. 1E). (1) Blocky surface loess, 0–1.40 m below surface. (2) Coarse, poorly to moderately well-sorted alluvial gravel and cobbles with clasts to 25 cm, 1.40–4.10 m. Angular to sub-angular cobbles moderately bedded with occasional finely bedded sand lenses containing scattered small gravel. Involutions (not shown), averaging 40 cm thick and containing some possible aeolian deposits, occur in the middle of the unit. An OSL sample was collected from within a sand lens in the lower portion of the unit 3.80 m below the surface. (3a) Coarse, well-sorted sand containing broken shell, possibly beach sand, 4.10–4.28 m. (3b) Ripple laminated silty clay, possible lagoonal deposits, 4.28–4.30 m. (3c) Sandy near-shore deposits consisting of ripple laminated clayey silt at base, coarsening upwards to fine sands. Ripple laminae disappear towards top, 4.30–5.00 m. An OSL sample was collected from 20 cm below the top of the unit, 4.70 m below the surface. (3d) Medium to well-sorted sands containing shell fragments, possibly beach sand, 5.00–5.15 m. (3e) Laminated silty sand to unknown depth, 5.15 to >5.35 m.

lacustrine deposition. A sand stringer within the basal deposits produced an OSL age of ~94.5 ka (Table 1). Clast on clast deposition unsupported by matrix occurs in a number of places and the unit may be the result of lacustrine deposition. However, the exposure is too limited to rule out an alluvial/fluvial origin. The surface of these lower gravels is truncated by small channels and rills. Two episodes of aeolian deposition overlie and fill these undulations. An OSL date of ~25.0 ka on a sample from the lower unit provides a limiting age for initiation of aeolian deposition. These deposits, along with the adjoining high surfaces of the lower gravels into which they are inset, were eroded to a level surface marked by an unconformity; a basal remnant of a moderately well-developed paleosol is visible in the loess below this unconformity. Post-glacial and Holocene loess deposited above the erosional unconformity form the surface deposits throughout the Qinghai Lake basin. An OSL sample at the base of this upper loess produced an age estimate of ~16.3 ka, consistent with previously reported ages for the initiation of loess deposition (Porter et al., 2001).

Given the ages of ~94 and ~102 ka for lagoonal deposits at ~3240 m (+46 m) on both the north and the south shore of the lake, an age of ~95 ka on possible lacustrine deposits at 3205–3210 m (+11–16 m) on the southwestern lake shore, and the absence of lacustrine deposits dating between ~95 and 25 ka at the same locale, we conclude that lake highstands at 20–66 m above the modern lake are likely MIS 5 in age.

## Low elevation paleoshorelines, 3194–3206 m

Multiple shorelines below ~3206 m (+12 m) apparently post-date the LGM with the maximum post-glacial lake elevation 9.5–12 m higher than present (Chen et al., 1990; Lister et al., 1991). This estimate was based, in part, on a section of aeolian sediments containing several soils at 3207 m (+13 m) (Chen et al., 1990). Basal radiocarbon dates of ~18.1 and ~12.9 cal ka suggest that these loess deposits span most of the terminal Pleistocene and Holocene.

Evidence for lake excursions during the Holocene is constrained by well-dated evidence of post-glacial and Holocene loess deposition and archaeological deposits. The surface loess exposed in numerous localities throughout the basin above ~3202 m was apparently deposited throughout the Holocene, interrupted by relatively stable periods of soil formation, but not by any evident lake highstands. Below ~3202 m the Holocene loess is largely or entirely removed, suggesting that mid- to late-Holocene lake activity higher than present is largely restricted to below this elevation. Two exposures near Heimahe (Fig. 1G) contain archaeological sites within post-glacial and Holocene loess. At Heimahe #1 (36.7304°N, 99.7699°E), elevation ~3210 m (+16 m), multiple AMS radiocarbon dates on charcoal stringers and hearth charcoal ~2.5 m below the surface range between 11.5 and 11.1 $^{14}$C ka BP (13.4–13.0 cal ka) (Madsen et al., 2006). At Heimahe #3 (36.7239°N, 99.7803°E), a hearth within the Holocene loess at ~3202–3 m dates to 7.6 $^{14}$C ka BP (~8.4 cal ka) (Rhode et al., 2007). A thin stringer of coarse sand containing broken shell fragments ~50 cm below this hearth may represent either a brief lake transgression or a stream flood event.

Given the shoreline geomorphology and these chronometric dates, we conclude Qinghai Lake fluctuated below ~3206 m (+12 m) during the post-glacial period, not exceeding ~3202–3 m after ~8.4 ka.

## Summary and discussion

Based on these data, we suggest a revised Qinghai Lake shoreline history that excludes significant late Pleistocene highstands >66 m above modern levels (Fig. 8). Lake highstands between ~20 and 66 m above modern are considerably older than previously thought and may include a transgressive lake at 3240 m (+46 m) ~110–90 ka (late MIS 5), eventually reaching ~3260 m (+66 m). We recognized no geomorphic evidence of a high lake stand above ~3260 m during the late Pleistocene, although a highstand at a much earlier age cannot be ruled out.

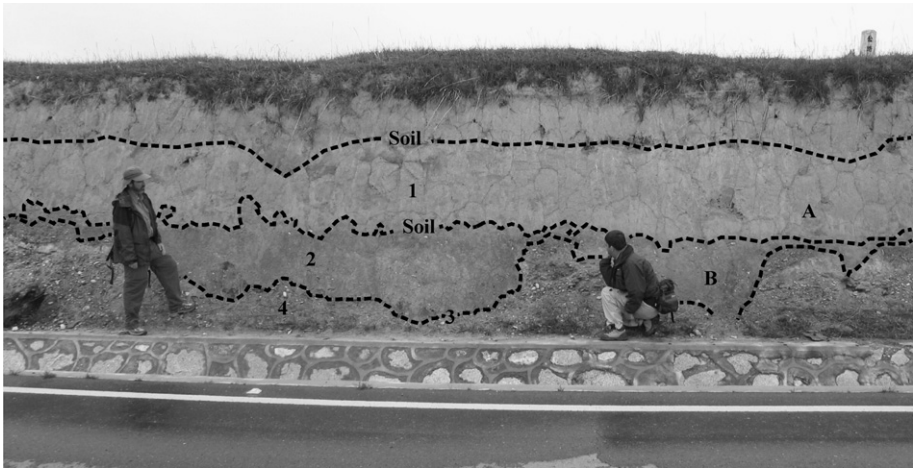


Figure 7. Southwest lake margin road cut at ~3207 m (+13 m above modern lake) (36.7588°N, 99.7713°E; Fig. 1F). (1) 2–2.2 m of loess containing at least one major visible soil. This upper loess fills small (20–40 cm deep) ice/sand wedge casts in underlying sediments ("A" above). (2) Lower aeolian sandy silt filling small channels or rills and cryogenic features in the surface of the underlying sandy gravels. Where these channels are particularly large this aeolian deposit reaches a maximum of 1.3 m thick. An erosional unconformity on the top of this aeolian material extends across the top of the underlying sediments between the rills. A stone line and a moderately well-developed soil are formed on this surface. This lower aeolian deposit fills cryogenic ice/sand wedge casts that penetrate the underlying gravel unit and the soil formed on it ("B" above). An OSL sample from 20 cm above the base of this unit and 2.25 m below the surface dates to ~25.0 cal ka. (3) Small channels or rills in soliflucted sands and gravels with rises and swales. The rises are spaced 2–5 m apart with the swales averaging 0.8–1.0 m deep. The swales appear to have been formed by rills truncating the lower horizontally bedded lacustrine/fluvial deposit. (4) Sandy gravels and cobbles with some internal layering evident. The exposure is limited and the gravels may represent either alluvial/fluvial deposits or wave-reworked materials. The cobbles are rounded to sub-angular and mostly platy in shape. The rises contain jumbled clasts with a matrix of yellow silt and sand; some unfilled pockets are also present, lacking matrix. Some evidence of imbrication is present. The maximum clast size is 5–7 cm diameter, with some to 10 cm. The underside of the clasts is coated with a stage 2 carbonate layer. Mantling this jumbled-clast layer is a thin unit of finer grained coarsely banded sands and silts, the particles coated with clay skins. On top of this sand and silt layer is an armoring layer of gravels and sands oriented parallel to the surface of the channel. This gravel armor is reddened with soil development. This soil forms a composite soil on the rises at the erosional unconformity on the top of the lower loess. On top of the rises cryogenic ice/sand wedge casts filled with the overlying aeolian sandy silt penetrate this soil. An OSL sample dating to 94.5 cal ka was collected from a sand lens in this unit in an adjacent road cut 2.90 m below the surface.

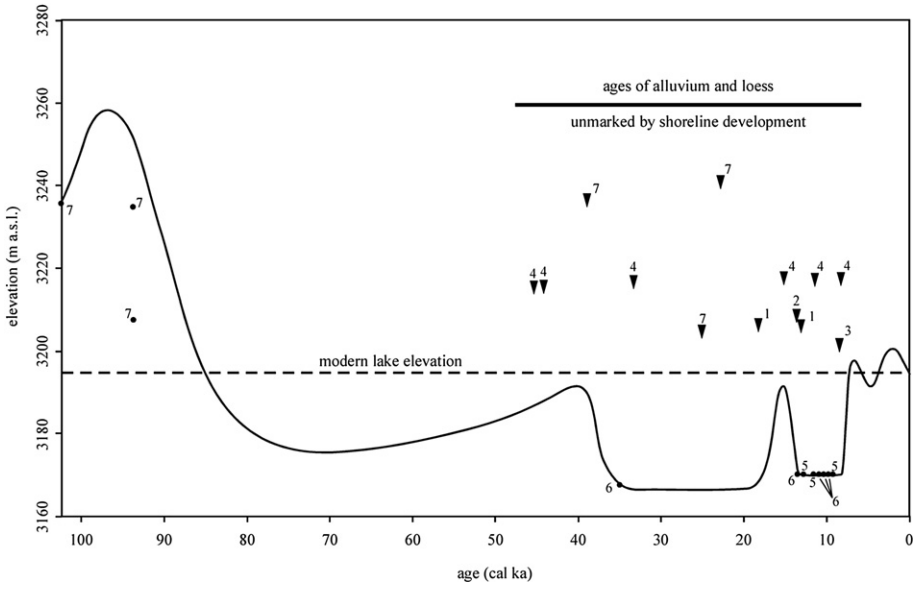


Figure 8. Schematic shoreline history for Qinghai Lake for the last ~100 ka plotted against age estimates for shoreline elevations. We consider this reconstruction tentative, with refinements likely to be made, but consider the general relationships to be reliable. Dots represent samples from sediments deposited at or near the lake surface. Samples from below the modern surface are derived from $^{14}C$ age estimates run on *Rupia* sp. seeds retrieved from sediment cores. *Rupia* grows in shallow water, generally less than 1 m deep. However, these dates are from cores taken in an eastern sub-basin of the lake and the surface elevation of the western sub-basin fed by the Buha River may have been somewhat higher. Triangles represent the age and elevations of samples from alluvium and loess deposited when the lake surface must necessarily have been below these points. Age estimates from non-lacustrine sediments above 3260 m and from locations for which the depositional context is unclear are not included. Numbers refer to data sources: (1) Chen et al. (1990); (2) Madsen et al. (2006) [this represents an average of three $^{14}C$ age estimates]; (3) Rhode et al. (2007); (4) Porter et al. (2001) [the actual elevation for these samples is ~3215–3220 m, not 3305 m as originally published]; (5) Lister et al. (1991); (6) Yu (2005); (7) this paper.

Alluvium dating to ~45–18 ka that is unmarked by shoreline development, core data suggesting low lake elevations after ~35 ka (and possibly after ~70 ka), and the absence of lake deposits in low elevation exposures dating ~95 to ~25 ka together indicate that lake level rises during the MIS 3, late glacial termination, and the Holocene climatic optimum was modest in comparison to earlier highstands. However, the work reported here is preliminary and higher MIS 3 shorelines, obscured by later alluvium and/or erosion, may yet be found.

The lake highstands at 3240–3260 m suggest a dramatically different hydrologic balance in the Qinghai basin prior to ~45 ka, or more likely ~90 ka, than has prevailed more recently. Modeling suggests that annual precipitation must have been at least 200 mm greater than at present (>150% modern) to sustain a lake of this size in the Qinghai basin (Qin and Huang, 1998). Better age control for these highstands is still required, but if they are MIS 5 in age, a strengthened East Asian monsoon during that time (Yuan et al., 2004; Johnson et al., 2006) must have brought much more precipitation to the northeast Tibetan Plateau than during later MIS 3 and Holocene monsoon peaks (Yang et al., 2004).

This reconstructed Qinghai Lake shoreline history is consistent with a well-dated sediment and ostracod record from a nearby alpine lake (Herzschuh et al., 2005; Mischke et al., 2005), with lake histories further south in Yunnan (Hodell et al., 1999), and with local loess records spanning the same time period (Lu et al., 2004a,b; Vandeberghe et al., 2006). The Lake Luanhaizi record from the northeastern Qilian Shan suggests desiccation prior to ~45 cal ka and during the LGM, and a relatively shallow lake during MIS 3, with the deepest levels occurring during the post-glacial period (Herzschuh et al., 2005; Mischke et al., 2005). Like the Qinghai Lake shoreline history, the record also suggests limited glaciation in the Qilian Shan during MIS 2 and 3.

Other regional indications of high lake levels during MIS 3 contrast with this revised chronology, however (Chen and Bowler, 1986; Fang, 1991; Owen et al., 2006). A large lake fed by water from the northeastern Qilian Shan in what is now the Tengger Desert dates to MIS 3 (Zhang et al., 2004), but surface morphology suggests that it overflows into the Yellow River at elevations above the MIS 3 maximum and drainage precipitation may have been much higher during MIS 5. Periods of high lakes and increased alluviation in the Qaidam basin are thought to be coeval during MIS 3 (Owen et al., 2006), but this dating is based, in part, on previous interpretations of the Qinghai Lake sequence, and alluvial stratigraphy at Qinghai Lake clearly shows that the period of maximum alluviation *followed* a period of high lakes, regardless of chronological issues.

The asynchronous response of Qinghai Lake and other regional lakes to late-Pleistocene climate forcing may reflect substantial differences in the water balance of their basins driven by the same factors responsible for the asynchronous glaciation of the Tibetan Plateau (Benn and Owen, 1998). Northwest movement of the East Asian summer monsoon, resulting in some higher lake stands in northwest China during MIS 3, may not have extended onto the mid-elevation northeastern Tibetan Plateau. Although there was a heightened summer monsoon during MIS 3, it did not reach the level of the Holocene climatic optimum (Herzschuh, 2006; Owen et al., 2006), and strengthened westerlies may have kept monsoon precipitation restricted to more southern areas (Benn and Owen, 1998; Morrill et al., 2003; Sheppard et al., 2004; Lehmkuhl and Owen, 2005; Shen et al., 2005; Herzschuh, 2006; Vandeberghe et al., 2006). Glaciation in the Qilian Mountains was not significant enough at any time after MIS 5 to drive extensive meltwater expansions of the lake. However, this revised Qinghai Lake history does help confirm suggestions of increased Tibetan glaciation during the early part of the last glacial cycle relative to the last 50 ka (Lehmkuhl and Owen, 2005).

We consider the chronological aspects of this reconstruction to be preliminary due to the limitations of the dating techniques involved and to the inherent difficulty in defining shoreline histories of very ancient lakes. Lake Bonneville, in western North America, for example, has been extensively studied for over a century and hundreds of age estimates are available for interpretation, yet its shoreline history continues to be revised (e.g., Godsey et al., 2005; Oviatt et al., 2005). We consider an age estimate of >90 ka for the Qinghai Lake highstands at 3240–3260 m to be the most parsimonious explanation for a synthesis of core data, shoreline geomorphology, and available dates, but an age of as late as ~45 ka cannot be ruled out. The lack of a late Quaternary highstand above 3260 m (+56 m) and a lake fluctuating below ~3215 m (+21 m) after ~45 ka is more definitive.

## Acknowledgments

This research was supported by the US National Science Foundation (INT-0214870), the Wenner-Gren Foundation, the Sante Fe Institute, the University of California Los Angeles, the Desert Research Institute, the University of Arizona, the Mercyhurst Archaeological Institute, and the University of Texas, USA, and by the Qinghai Institute of Salt Lakes, Chinese Academy of Science, PRC.

## References

Aitken, M.J., Bowman, S.G.E., 1975. Thermoluminescent dating: Assessment of alpha particle contribution. Archaeometry 17, 132–138.

Balescu, S., Lamothe, M., 1992. The blue emission of K-feldspar coarse grains and its potential for overcoming TL age. Quaternary Science Reviews 11, 45–51.

Benn, D.I., Owen, L.A., 1998. The role of the Indian summer monsoon and the mid-latitude westerlies in Himalayan glaciation: Review and speculative discussion. Journal of the Geological Society 155, 353–363.

Chen, K., Bowler, J.M., 1986. Late Pleistocene evolution of salt lakes in the Qaidam Basin, Qinghai Province, China. Palaeogeography, Palaeoclimatology, Palaeoecology 54, 87–104.

Chen, K.Z., Bowler, J.M., Kelts, K., 1990. Paleoclimatic evolution within the Qinghai-Xizang (Tibet) Plateau in the last 40,000 years. Quaternary Science 1, 21–31 (in Chinese).

Fang, J.Q., 1991. Lake evolution during the past 30,000 years in China, and its implications for environmental change. Quaternary Research 36, 37–60.

Forman, S.L., Pierson, J., 2002. Late Pleistocene luminescence chronology of loess deposition in the Missouri and Mississippi river valleys, United States. Palaeogeography, Palaeoclimatology, Palaeoecolology 186, 25–46.

Geological Survey of Qinghai Province, 1991. Geological Memoir Series 1, 24. Geological Publishing House, Beijing (in Chinese).

Godsey, H.S., Currey, D.R., Chan, M.A., 2005. New evidence for an extended occupation of the Provo shoreline and implications for regional climate

change, Pleistocene Lake Bonneville, Utah, USA. Quaternary Research 63, 212–223.
Herzschuh, U., 2006. Palaeo-moisture evolution at the margins of the Asian monsoon during the last 50 ka. Quaternary Science Reviews 25, 163–178.
Herzschuh, U., Zhang, C., Mischke, S., Herzschuh, R., Mohammadi, F., Mingram, B., Kürschner, H., Riedel, F., 2005. A late Quaternary lake record from the Qilian Mountains (NW China), evolution of the primary production and the water depth reconstructed from macrofossil, pollen, biomarker and isotope data. Global and Planetary Change 46, 361–379.
Herzschuh, U., Kürschner, H., Mischke, S., 2006. Temperature variability and vertical vegetation belt shifts during the last ~50,000 yr in the Qilian Mountains (NE margin of the Tibetan Plateau, China). Quaternary Research 66, 133–146.
Hodell, D.A., Brenner, M., Kanfoush, S.L., Curtis, J.H., Stoner, J.S., Xueliang, S., Yuan, W., Whitmore, T.J., 1999. Paleoclimate of Southwestern China for the Past 50,000 yr Inferred from Lake Sediment Records. Quaternary Research 52, 369–380.
Hong, Y.T., Hong, B., Lin, Q.H., Zhu, Y.X., Shibata, Y., Hirota, M., Uchida, M., Leng, X.T., Jiang, H.B., Xu, H., Wang, H., Yi, L., 2003. Correlation between Indian Ocean summer monsoon and North Atlantic climate during the Holocene. Earth and Planetary Science Letters 211, 317–380.
Jain, M., Botter-Jensen, L., Singhvi, A.K., 2003. Dose evaluation using multiple-aliquot quartz OSL: Test of methods and a new protocol for improved accuracy and precision. Radiation Measurements 37, 67–80.
Ji, J., Shen, J., Balsam, W., Chen, J., Liu, L., Liu, X., 2005. Asian monsoon oscillations in the northeastern Qinghai-Tibet Plateau since the late glacial as interpreted from visible reflectance of Qinghai Lake sediments. Earth and Planetary Science Letters 233, 61–70.
Johnson, K.R., Ingram, B.L., Sharp, W.D., Zhang, P., 2006. East Asian summer monsoon variability during Marine Isotope Stage 5 based on speleothem $\delta^{18}O$ records from Wanxiang Cave, central China. Palaeogeography, Palaeoclimatology, Palaeoecology 236, 5–19.
Lang, A., Hatte, C., Rousseau, D.-D., Antoine, P., Fontugne, M., Zoller, L., Hambach, U.A., 2003. High-resolution chronologies for loess: Comparing AMS $^{14}C$ and optical dating results. Quaternary Science Reviews 22, 953–959.
Lanzhou Institute of Geology, 1979. Qinghai Lake monograph, 1961 expedition. Science Press Series, Beijing (in Chinese).
Lehmkuhl, F., Owen, L.A., 2005. Late Quaternary glaciation of Tibet and the bordering mountains: A review. Boreas 34, 87–100.
Lister, G.S., Kelts, K., Chen, K.Z., Yu, J.-Q., Neissen, F., 1991. Lake Qinghai, China: Closed-basin lake levels and the oxygen isotope record for ostracoda since the latest Pleistocene. Palaeogeography, Palaeoclimatology, Palaeoecology 84, 141–162.
Liu, X., Shen, J., Wang, S., Yang, X., Tong, G., Zhang, E., 2002. A 16,000-year pollen record of Qinghai Lake and its paleoclimate and palaeoenvironment. Chinese Science Bulletin 47, 1931–1936.
Lu, H., Wang, X., Ma, H., Tan, H., Vandenberghe, J., Mial, X., Li, Z., Sun, Y., An, Z., Cao, G., 2004a. The plateau monsoon variation during the past 130 kyr revealed by loess deposit at northeast Qinghai-Tibet (China). Global and Planetary Change 41, 207–214.
Lu, H., Vandenberghe, J., Miao, X., Tan, H., Ma, H., 2004b. Evidence for an abrupt climatic reversal during the Last Interglacial on the northeast Qinghai-Tibetan Plateau. Quaternary International 154–155, 136–140.
Madsen, D.B., Ma, H., Brantingham, P.J., Gao, X., Rhode, D., Zhang, H., Olsen, J.W., 2006. The late Upper Paleolithic occupation of the northern Tibetan Plateau margin. Journal of Archaeological Science 33, 1433–1444.
Mischke, S., Herzschuh, U., Zhang, C., Bloemendal, J., Riedel, F., 2005. A Late Quaternary lake record from the Qilian Mountains (NW China): Lake level and salinity changes inferred from sediment properties and ostracod assemblages. Global and Planetary Change 46, 337–359.
Morrill, C., Overpeck, J.T., Cole, J.E., 2003. A synthesis of abrupt changes in the Asian summer monsoon since the last deglaciation. Holocene 13, 465–476.
Oviatt, C.G., Miller, D.M., McGeehin, J.P., Zachary, C., Mahan, S., 2005. The Younger Dryas phase of Great Salt Lake, Utah, USA. Palaeogeography, Palaeoclimatology, Palaeoecology 219, 263–284.
Owen, L.A., Finkel, R.C., Ma, H., Barnard, P.L., 2006. Late Quaternary landscape evolution in the Kunlun Mountains and Qaidam Basin, Northern Tibet: A framework for examining the links between glaciation, lake level changes and alluvial fan formation. Quaternary International 154–155, 73–86.
Pan, B., 1994. Research upon the geomorphologic evolution of the Guide Basin and the development of the Yellow River. Arid Land Geography 7, 43–50 (in Chinese).
Porter, S.C., Singhvi, A., An, Z., Lai, Z., 2001. Luminescence age and palaeoenvironmental implications of a late Pleistocene ground wedge on the northeastern Tibetan Plateau. Permafrost and Periglacial Processes 12, 203–210.
Prescott, J.R., Hutton, J.T., 1994. Cosmic ray contributions to dose rates for luminescence and ESR dating: Large depths and long-term time variations. Radiation Measurements 23, 497–500.
Qin, B., Huang, Q., 1998. Evaluation of the climatic change impacts on the inland lake—A case study of Lake Qinghai, China. Climatic Change 39, 695–714.
Rhode, D., Zhang, H., Madsen, D.B., Gao, X., Brantingham, P.J., Ma, H., Olsen, J.W., 2007. Epipaleolithic/early Neolithic settlements at Qinghai Lake, western China. Journal of Archaeological Science 34, 600–612.
Shen, J., Liu, X., Wang, S., Matsumoto, R., 2005. Palaeoclimatic changes in the Qinghai Lake area during the last 18,000 years. Quaternary International 136, 131–140.
Sheppard, P.R., Tarasov, P.E., Graumlich, L.J., Heussner, K.-U., Wagner, M., Österle, H., Thompson, L.G., 2004. Annual precipitation since 515 BC reconstructed from living and fossil juniper growth of northeastern Qinghai Province, China. Climate Dynamics 23, 869–881.
Vandeberghe, J., Renssen, H., van Huissteden, K., Nugteren, G., Konert, M., Lu, H., Dodonov, A., Buylaert, J.-P., 2006. Penetration of Atlantic westerly winds into Central and East Asia. Quaternary Science Reviews 25, 2380–2389.
Wang, S.M., Li, J.R., 1991. Lacustrine sediments—An indicator of historical climatic variation, the case of Lakes Qinghai and Daihai. Chinese Science Bulletin 36, 1364–1368 (in Chinese).
Wang, S.M., Shi, Y.F., 1992. Review and discussion on the late Quaternary evolution of Qinghai Lake. Journal of Lake Sciences 4, 1–10 (in Chinese).
Wang, S.M., Wang, Y.F., Wu, R.J., Li, J.R., 1991. Qinghai Lake level fluctuation and climatic change since the last glaciation. Chinese Journal of Oceanology and Limnology 9, 179–183 (in Chinese).
Yang, B., Shi, Y., Braeuning, A., Wang, J., 2004. Evidence for a warm–humid climate in arid northwestern China during 30–40 ka BP. Quaternary Science Reviews 23, 2537–2548.
Yu, J.Q., 2005. Lake Qinghai, China: A multi-proxy investigation on sediment cores for the reconstructions of paleoclimate and paleoenvironment since the Marine Isotope Stage 3. Dissertation, Faculty of Materials and Geoscience, Technical University of Darmstadt.
Yu, J.Q., Kelts, K.R., 2002. Abrupt changes in climate conditions across the late-glacial/Holocene transition on the N.E. Tibet-Qinghai Plateau: Evidence from Lake Qinghai, China. Journal of Paleolimnology 28, 195–206.
Yuan, B.Y., Chen, K., Ye, S.J., 1990. Origin and evolution of Lake Qinghai. Quaternary Sciences 3, 233–243 (in Chinese).
Yuan, D., Cheng, H., Edwards, R.L., Dykoski, C.A., Kelly, M.J., Zhang, M., Qing, J., Lin, J., Wang, Y., Wu, J., Dorale, J.A., An, Z., Cai, Y., 2004. Timing, duration, and transitions of the last interglacial Asian monsoon. Science 23, 575–578.
Zhang, H.C., Peng, J.L., Ma, Y.Z., Chen, G.J., Feng, Z.D., Li, B., Fan, H.F., Chang, F.Q., Lei, G.L., Wünnemann, B., 2004. Late Quaternary palaeolake levels in Tengger Desert, NW China. Palaeogeography, Palaeoclimatology, Palaeoecology 211, 45–58.